

Multi-depth valved microfluidics for biofilm segmentation

This content has been downloaded from IOPscience. Please scroll down to see the full text.

2015 J. Micromech. Microeng. 25 095003

(<http://iopscience.iop.org/0960-1317/25/9/095003>)

View [the table of contents for this issue](#), or go to the [journal homepage](#) for more

Download details:

IP Address: 206.196.186.155

This content was downloaded on 01/09/2015 at 19:07

Please note that [terms and conditions apply](#).

Multi-depth valved microfluidics for biofilm segmentation

M T Meyer^{1,2}, S Subramanian^{2,3}, Y W Kim^{2,3}, H Ben-Yoav², M Gnerlich²,
K Gerasopoulos^{2,3}, W E Bentley¹ and R Ghodssi^{1,2,3}

¹ Fischell Department of Bioengineering, University of Maryland, College Park, MD, 20742, USA

² Institute for Systems Research, University of Maryland, College Park, MD, 20742, USA

³ Department of Electrical and Computer Engineering, University of Maryland, College Park, MD, 20742, USA

E-mail: ghodssi@umd.edu

Received 25 April 2015, revised 16 June 2015

Accepted for publication 17 June 2015

Published 6 August 2015



CrossMark

Abstract

Bacterial biofilms present a societal challenge, as they occur in the majority of infections but are highly resistant to both immune mechanisms and traditional antibiotics. In the pursuit of better understanding biofilm biology for developing new treatments, there is a need for streamlined, controlled platforms for biofilm growth and evaluation. We leverage advantages of microfluidics to develop a system in which biofilms are formed and sectioned, allowing parallel assays on multiple sections of one biofilm. A microfluidic testbed with multiple depth profiles was developed to accommodate biofilm growth and sectioning by hydraulically actuated valves. In realization of the platform, a novel fabrication technique was developed for creating multi-depth microfluidic molds using sequentially patterned photoresist separated and passivated by conformal coatings using atomic layer deposition. Biofilm thickness variation within three separately tested devices was less than 13% of the average thickness in each device, while variation between devices was 23% of the average thickness. In a demonstration of parallel experiments performed on one biofilm within one device, integrated valves were used to trisect the uniform biofilms with one section maintained as a control, and two sections exposed to different concentrations of sodium dodecyl sulfate. The technology presented here for multi-depth microchannel fabrication can be used to create a host of microfluidic devices with diverse architectures. While this work focuses on one application of such a device in biofilm sectioning for parallel experimentation, the tailored architectures enabled by the fabrication technology can be used to create devices that provide new biological information.

Keywords: atomic layer deposition, polydimethylsiloxane, microfluidics, hydraulically actuated valve, bacterial biofilm

 Online supplementary data available from stacks.iop.org/JMM/25/095003/mmedia

(Some figures may appear in colour only in the online journal)

1. Introduction

Bacterial biofilms are a persistent health problem. Characterized by a threshold population of bacteria surrounded by a self-secreted extracellular matrix, biofilms are challenging to eliminate once formed. Host immune mechanisms are often ineffective against biofilms, as biofilms have been shown to

impede phagocytosis as well as penetration of leukocytes into their structure [1, 2]. Within biofilms, high rates of mutation and horizontal exchange of genetic material promote selection of antibiotic tolerance mechanisms [2, 3]. Unfortunately, biofilms occur in the majority of clinical infections, commonly forming on catheters, prosthetic joints, respiratory tract surfaces, and teeth [4]. In the pursuit of understanding bacterial

biofilms, a number of *in vitro* models have been developed [5–8]. However, just as each clinically observed infection is unique, biofilms grown *in vitro* also show variability within and between platforms [9, 10]. Variability between platforms precludes reliable comparison of biofilms under experimental conditions to biofilms under control conditions. Frequently, macroscale biofilm experiments will address these variations by forming a biofilm within one reactor, either on a continuous surface such as a catheter, or on individual coupons within the reactor [5, 11, 12]. The surface can then be segmented so that individual sections can be tested for biofilm characteristics and sensitivity.

The rapidly expanding field of microfluidics has fostered development of myriad lab-on-a-chip technologies ranging from gene expression assays [13] to cell and tissue culture [14, 15]. Advantages of microscale fluidic systems over macroscale technologies vary depending on the application, but often include the use of smaller sample volumes, a tighter control of the physical and chemical microenvironment, and the ability to integrate microscale sensors with fluidic handling, enabling real-time sensing and sensor feedback. These properties of microfluidics provide a significant advantage over traditional biofilm growth platforms such as macroscale flow cells and 96 well microplate-based devices; by shrinking the growth volume, the microenvironment of biofilms can be more tightly controlled within microfluidics. A smaller volume also minimizes the amount of reagent used within each study, maximizing the amount of information that can be gathered using a small volume of a reagent such as a stain, antibody, or drug under development. While studies of biofilms and of microfluidics have existed for decades, recently the two fields have merged and spawned research providing new insight on physical robustness of biofilms [16], roles of intercellular communication [17–21], and development of antibiotic resistance [22, 23] among other topics [24].

Once the biofilm has formed in a microchannel, variability between devices still exists, as with macroscale biofilms [9, 25]. Performing different tests on separate portions of one biofilm provides an advantage over parallel biofilm formation, as the variability between biofilms formed in separate devices can preclude their accurate comparison when used as experimental and control groups in a biofilm assay. One method of addressing variability at the microscale is performing experiments on parallel biofilms grown in separate channels sharing a common inlet [17, 19]. However, in order to eliminate the possibility of cross-contamination between biofilm assays, it would be ideal to adapt the macroscale approach of physical biofilm segmentation for integration into a microfluidic biofilm growth platform. To the best of the authors' knowledge, partitioning one biofilm into several testable sections in a microfluidic setting has not been reported.

Within the field of microfluidics, valves are commonly used for controlling fluid flow within a device. There are many configurations of valves, such as implementation of external pins or solenoids [26, 27] to compress a fluidic channel embedded in the flexible silicone polydimethylsiloxane (PDMS). Integrating valves into the PDMS itself and using a pressurized gas [19, 28, 29] to control the valve orientation

is a popular valving scheme used in much of today's microfluidic work. As opposed to externally actuated pins or solenoids, these types of integrated valves are convenient for imaging microfluidic channel contents, as using only an in-plane gas line for valve actuation maintains an open line of sight for optimal characterization of channel contents via microscopy. Valves created using this method are typically able to seal channels up to a certain depth, on the order of tens of microns, dependent on the aspect ratio of the channel, the material properties of the PDMS used, and the valve style [28]. Conversely, in order to obtain microfluidic biofilms with sufficient structure and maturity for response evaluation, microfluidic channels are typically constructed with depths of at least $100\mu\text{m}$ so that the amount of shear stress imposed upon the biofilm does not delaminate the structure or prevent biofilm maturation. The differing depth requirements of PDMS valves and biofilm growth within microfluidics may be addressed, as in this work, by fabricating multi-depth microfluidic channels that are shallow in the valve regions and deep in areas for biofilm growth.

Photoresist structures may be patterned on top of a rigid substrate and used directly for molding PDMS [30]. While several iterations of depositing and patterning one or multiple types of photoresist may create multiple heights on one wafer, preserving a photoresist pattern throughout subsequent lithography cycles often proves challenging. In this work, the incompatibilities presented by patterning multiple layers of photoresists are avoided by implementing a passivation layer of Al_2O_3 deposited via atomic layer deposition (ALD). ALD is capable of creating high quality, thin, conformal layers of a multitude of materials at low temperatures [31, 32]. While ALD-deposited materials have been used on photoresist as an etch mask [33] or as a layer to be patterned by liftoff [34, 35], to the best of the authors' knowledge ALD has not been implemented in creating a chemical and structural passivation layer for photoresist.

We present a device designed to segment bacterial biofilms in one microfluidic channel for multiplexed experiments. Sectioning is achieved by integrating hydraulically actuated valves into the PDMS microfluidic device. The differing depth requirements of PDMS valves (shallow, rounded) and biofilm growth (deep) are negotiated by creating a mold with two types of photoresist. Fabrication incompatibilities between resist types are circumvented by passivating pre-existing photoresist structures using ALD. The final device was implemented in a successful demonstration of biofilm growth and segmentation, and used to evaluate the effects of different concentrations of the surfactant sodium dodecyl sulfate (SDS) on mature biofilms.

2. Methods

2.1. Device design

The valved device includes one set of microfluidic channels where biofilms grow and are controlled, and another set of microfluidic channels for operating valves that manipulate the biofilms. An overview of the device operation is depicted

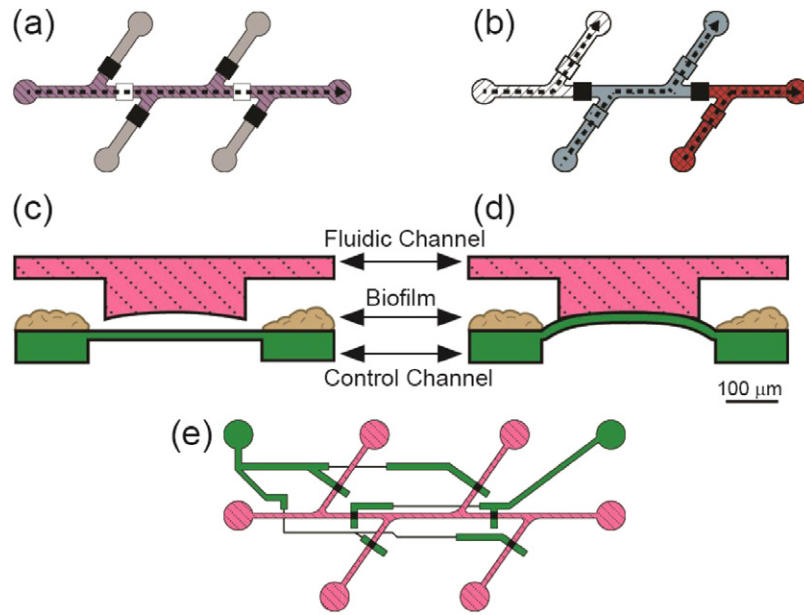


Figure 1. (a) Schematic of device operation during biofilm growth, with side channels blocked by closed valves (solid black squares) (b) Device operation during biofilm sectioning, with side channels open and central channel trisected by two closed valves (c) Side-view schematic of open push-up valve integrated with two-depth channel (d) Side-view schematic of closed push-up valve with pressure applied to the control channel to close the valve (e) Mask layout for PDMS molds. Pink channels denote the top, biofilm-containing layer, and green channels denote the bottom, hydraulic control layer.

in figures 1(a) and (b). The device was designed to have one central microfluidic channel where biofilms form and mature, with access to side channels blocked by closed valves (figure 1(a)). After maturation, the central channel is divided into three sections using hydraulically actuated valves integrated in the PDMS structure. Valves that formerly blocked access to the side channels are opened, as shown in figure 1(b), to allow flow over each of the three sections of preformed biofilm.

In order to control the flow in a streamlined manner, hydraulically actuated ‘push-up’ style valves [28] were integrated in the two device layers of PDMS (figure 1(c)). Microchannels in the top layer contain biofilms and the surrounding media. The bottom layer contains channels covered by a thin PDMS membrane and filled with liquid, to which pressure is applied. In the valve area, this pressure deforms the membrane and presses it against the rounded ceiling of the top channel, thereby closing the valve (figure 1(d)).

The amount of membrane deflection relies on many factors, including the channel dimensions, PDMS thickness, and applied pressure [28]. The maximum deflection of a push-up-style valve is typically no more than $60\ \mu\text{m}$ [28]. The channel geometry, including its depth, is directly related to shear stress; the shear stress in turn affects biofilm growth properties, such as thickness and structure [12, 16, 18]. In this work, we maintained continuity with our previous work by maintaining a $100\ \mu\text{m}$ channel depth for biofilm growth, as altering the shear rate can affect the base state of the biofilm. As the integrated valves require a channel less than $60\ \mu\text{m}$ in height, it was necessary to design a compromise between the two depth requirements, as shown in figures 1(c) and (d). The top layer of PDMS contains channels that are mostly deep; in the areas to be sealed by valves, the channel profile is shallow and rounded, allowing for more complete sealing than a square

profile. In order to create valved, multi-depth channels, the control channel and membrane must be the bottom-most layer, as opposed to the top layer, with PDMS spun on-top of the control channel [29]; the fluidic channel is created by a mold with multiple heights, on top of which spinning a uniform PDMS membrane is difficult.

2.2. Fabrication

The channel profiles in both PDMS layers were created using photoresist molds patterned photolithographically on a silicon wafer. Schematics of the device layout indicating the mask layers used are shown in figure 1(e). The fluidic channels are $350\ \mu\text{m}$ wide, and the central channel through which biofilms are grown are $24\ \mu\text{m}$ long.

2.2.1. Molds for PDMS microfluidics. The mold for the bottom layer of PDMS containing the valve control channels is fabricated from a single, $35\ \mu\text{m}$ layer of Microchem KMPR 1050 patterned on a silicon wafer.

The mold for the top layer of PDMS, containing the two-depth channels where biofilms are grown, is fabricated according to the process depicted in figure 2. First, the shallow valve areas are defined in $22\ \mu\text{m}$ -thick AZ 9260. AZ 9260 was chosen as the resist for the valve areas due to its ability to be reflowed. After exposure and development, the resist is hardbaked on a hotplate at $175\ ^\circ\text{C}$ for 20 min to create the rounded profile. In order to prevent cracking due to large thermal gradients, the wafer is placed on a room temperature hotplate, and is allowed to remain there as it heats to the final bake temperature, during the hardbake, and after the hardbake as the hotplate naturally cools to room temperature. The high bake temperature also

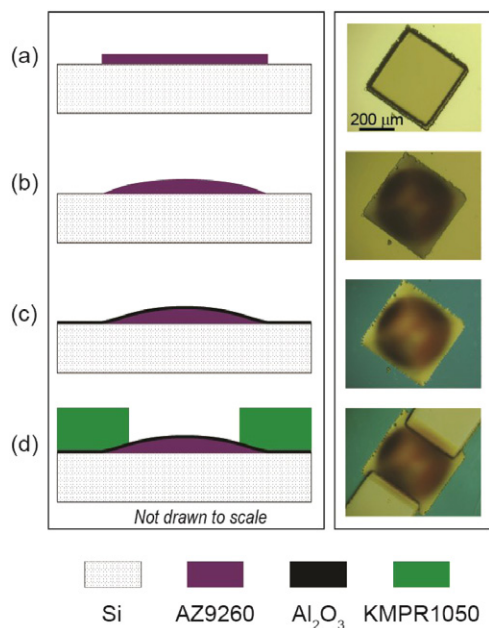


Figure 2. Cross-sectional schematics (not drawn to scale) and corresponding top-view photographs of fluidic mold fabrication: (a) patterning of AZ 9260 positive resist (22 μm), (b) resist rounding and hardbake at 175 °C for 20 min, (c) passivation with ALD Al₂O₃ (100 nm), and (d) KMPR 1050 patterning (100 μm).

drives out residual solvents in preparation for subsequent processing. After hardbaking, ALD is used to deposit a 100 nm layer of Al₂O₃ at 150 °C over the AZ 9260 pattern. As a result of the low temperature deposition process and resulting dense and conformal film, this layer protects the AZ 9260 pattern from interactions with solvents in subsequent processes without sacrificing the underlying form of the resist. A layer of 100 μm -thick KMPR 1050 is patterned on top of the Al₂O₃ barrier layer to form the mold for deep sections of the fluidic channel where biofilms grow. KMPR 1050 was used to mold the biofilm growth sections due to its suitability for creating thick, structural, photopatterned films. The KMPR 1050 could not be deposited prior to the AZ 9260, since the thick KMPR 1050 structures immediately adjacent to the rounded valve area obstruct the use of photolithography to pattern the AZ 9260 footprint and profile.

2.2.2. PDMS processing. Both molds are treated with a solution of Alconox[®] powdered precision cleaner prior to PDMS processing to prevent PDMS adhesion to the mold surface. Patterned wafers are immersed in a petri dish with 0.75% Alconox[®] detergent dissolved in deionized (DI) water for 2 min, removed, and allowed to air dry. PDMS (Sylgard 184, Dow Corning) prepared in a ratio of 20:1 (base: curing agent) is spun on top of the valve control channel mold to a final thickness of approximately 50 μm, creating approximately 15 μm-thin membranes at the valve areas (supplementary materials, figure S1) (stacks.iop.org/JMM/25/095003/mmedia). PDMS for the fluidic layer is prepared in a 5:1 ratio (base: curing agent) and poured over the fluidic mold. The PDMS-covered molds are cured in a furnace for 15 min

at 60 °C. The fluidic layer PDMS is peeled off its mold and cut into pieces corresponding to each fluidic device. Inlet and outlet holes are drilled into the fluidic layer PDMS with a 0.2 mm dermatological punch. The fluidic layer pieces are aligned to and placed on top of the hydraulic control layer still on its mold, and the stack is baked again in a furnace at 80 °C for 3 h. Due to the mismatch in PDMS component ratios in the two layers, the partially cured layers are bonded together during a long bake at this higher temperature [36]. PDMS stacks corresponding to each device are cut and peeled off the control channel mold. Holes for the control channel inlets are drilled through each stack, which is permanently bonded to a glass coverslip by exposing bonding surfaces to oxygen plasma for 30 s at 20 W and 400 mTorr. Bonded devices are baked in a furnace for 3 h at 60 °C to strengthen the bond.

2.3. Device preparation

Fluidic connections are made to the device as described in previous work [20]. 1/16" barbed tubing connectors were inserted into the inlet and outlet holes and connected with Tygon[®] tubing to either a syringe pump or a microcentrifuge tube serving as a waste reservoir. The hydraulic control channels are prepared for operation by pre-filling with deionized (DI) water mixed with a drop of standard food coloring. If these channels are not pre-filled with liquid, as pressure is applied to the channel via pressurized nitrogen, the gas diffuses through the thin PDMS membrane at the valves and reemerges in the fluidic channel as a bubble, interrupting flow and delaminating adherent biofilms. Tubing connected to the hydraulic control channel inlets is coupled to a filled syringe dispensing dyed DI water at a flow rate of 20 μL h⁻¹. As the control channels lack outlets, flow is stopped when dyed water is visually confirmed to have reached the ends of the channels. The tubing connected to the control channels is subsequently connected to a tank of controlled, pressurized nitrogen. To close valves, a nitrogen pressure of 15 psi is applied to the control channel controlling the valves to be closed. Valves are opened by releasing this pressure.

2.4. Operation: biofilm growth

Channels are sterilized in both device orientations by using a flow rate of 20 μL h⁻¹ to introduce 70% ethanol into the channels for 30 min. After rinsing the device with DI water at 20 μL h⁻¹ for 30 min, again for both orientations, the device is reverted to biofilm growth orientation as in figure 1(a).

A culture of *Escherichia coli* K-12 MG1655, grown overnight at 250 rpm and 37 °C, is diluted to an OD₆₀₀ of 0.25 in Lysogeny broth (LB) media and injected into the device just until the channel is filled. The suspension is incubated in the device under static conditions for 2 h in a 37 °C incubator to allow bacterial adhesion to the PDMS channel floor. With the device remaining in the incubator, flow of sterile LB growth media at 7.5 μL h⁻¹ is initiated after the incubation period and applied continuously for the set time period of biofilm growth.

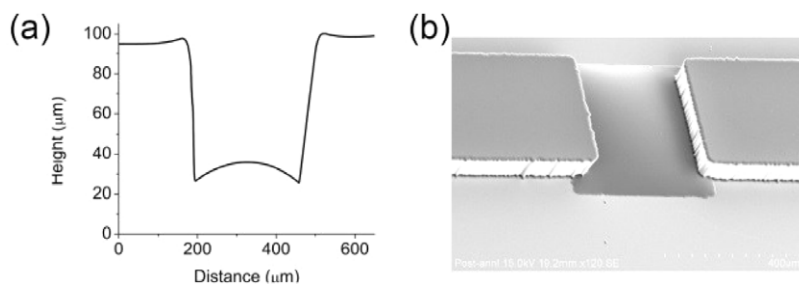


Figure 3. (a) Contact profilometry scan of mold at valve region, verifying the presence of the desired profiles. In the measured region, the rounded AZ 9260 section had a peak height of $36\mu\text{m}$, and the KMPR 1050 channels had a depth of approximately $97\mu\text{m}$. (b) SEM image of multi-depth structure created from two photoresists. Note the large difference in aspect ratios minimizes the appearance of curvature in the shallow section.

2.5. Operation: biofilm segmentation

In the presented biofilm segmentation studies, biofilms were grown as previously described. After the set period of biofilm growth time, the valve orientation was switched by releasing the pressure from the valves blocking the side channels, and applying pressure to the control channels controlling the valves in the central channel. Each section could then be exposed to treatment as shown in the schematic in figure 1(b); in this demonstration of the device's applicability to biofilm studies, two sections were exposed to two different SDS concentrations (0.1% and 0.2% in LB media) at $7.5\mu\text{Lh}^{-1}$ for one hour, and one section was maintained as a control via exposure to LB media at $7.5\mu\text{Lh}^{-1}$ for one hour.

2.6. Staining, confocal microscopy, image analysis

Biofilms were stained, imaged, and analyzed based on previously developed procedures [20, 21]. After biofilm formation or treatment, biofilms were rinsed with deionized water then stained with the Filmtracer™ LIVE/DEAD® Biofilm Viability Kit (Molecular Probes, Inc.), using equal proportions of SYTO9 and propidium iodide introduced into the biofilm-containing channels at a flow rate of $7.5\mu\text{Lh}^{-1}$. The biofilms were rinsed again with deionized water and imaged using confocal microscopy (Zeiss LSM 710). One spot was imaged in each of the three segments per device; images were obtained close to the center point of each segment, approximately 4 mm away from the valve areas. COMSTAT [37] was used to quantitatively analyze confocal image stacks and obtain average thickness, biomass, and substratum coverage values. Confocal image stacks were visualized using Imaris (Bitplane, Inc.). As the viability stain assay was not calibrated for biofilms formed within this platform, quantitative viability data is not presented here. JMP® statistical analysis software was used for all statistical calculations.

3. Results

3.1. Fabrication of multiple channel profiles and valve functionality

Deposition of a physical and chemical barrier via ALD proved a reliable method for patterning multiple resist formulations and profiles. Using the methods described above, a 100% yield of intact AZ 9260 was obtained repeatably. Successful patterning of the two photoresists to obtain the desired profiles is depicted

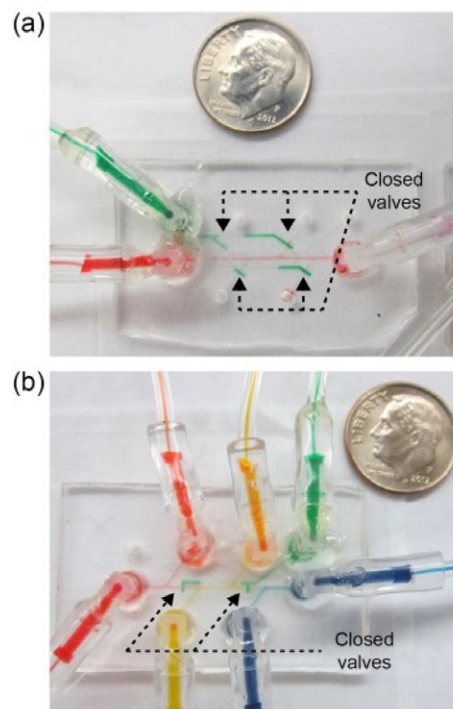


Figure 4. Photographs of assembled devices with green water filling actuated control channels. (a) Device in biofilm growth orientation, with side channels blocked by closed valves. Photograph corresponds to figure 1(a). (b) Device in biofilm sectioning orientation, with side channels open and central channel sectioned by closed valves. Photograph corresponds to figure 1(b).

by the profilometry data and scanning electron microscopy (SEM) image in figures 3(a) and (b). As shown, the KMPR 1050 was patterned to be $100\mu\text{m}$ thick, while the rounded AZ 9260 structure typically had a peak height of $35\mu\text{m}$.

Microfluidic devices fabricated from the two photoresist molds were assembled to form valved microfluidic channels. The functionality of the valves was confirmed by introducing flow of deionized water dyed with food coloring (figure 4 and supplementary material, figure S2) (stacks.iop.org/JMM/25/095003/mmedia).

3.2. Biofilm uniformity

In order to use the device for biofilm studies with integrated controls, biofilms grown in the central channel must be

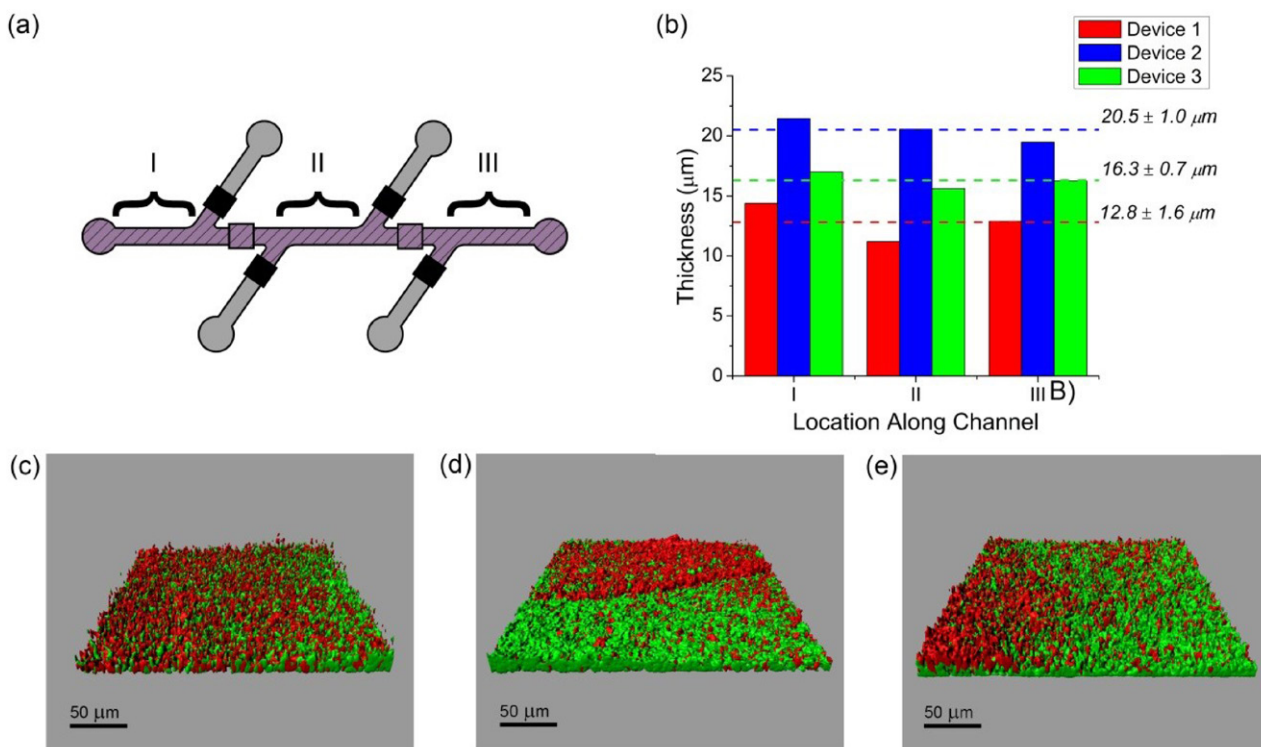


Figure 5. (a) Schematic of device operation during biofilm growth, with side channels blocked by closed valves. Confocal microscopy images were obtained at the center of each of the three sections indicated (I, II, and III) (b) Average biofilm thicknesses measured at imaged locations in the three devices tested. Locations were positioned in the center of each section, with section I closest to the inlet, and III closest to the outlet. Dashed lines indicate averaged thickness across imaged locations for each device. (c)–(e) Surface rendered confocal microscopy images from Device 3, Sections (c) I, (d) II, and (e) III. Thicknesses were 17.0, 15.6, and 16.2 μm respectively.

uniform so that upon segmentation, the control section may be compared to the experimental sections in good faith knowing that prior to segmentation, all sections were comparable. It was noted that the shallow valve regions do not become clogged with biofilm, and growth occurs on both sides of the open valve area as depicted in supplementary material, figure S3 (stacks.iop.org/JMM/25/095003/mmedia). The lack of bacterial growth within the valve region is hypothesized to be due to the increased amount of shear stress in the shallow, rounded sections of the channel as compared to the 100 μm-deep regions. Increased shear imposed on the biofilm within the valve region can reduce its thickness and can inhibit overall growth.

Uniformity was verified by growing *E. coli* biofilms in the central channel for 48 h, then staining, imaging, and analyzing the biofilm in each of the three segments. The segments are denoted as I, II, and III, corresponding to the segment closest to the inlet, the middle segment, and segment closest to the outlet respectively, as indicated in figure 5(a). Two of the devices, Devices 1 and 2 as shown in figure 5(b), were tested in parallel, while Device 3 was tested one month later. Results from the three devices tested are summarized in figure 5(b) and samples of rendered confocal microscopy images from one device are shown in figures 5(c)–(e).

The results show that biofilms have small thickness variations within each device, with standard deviations (SD) less than 2 μm, 13% of the average thickness at greatest.

Comparatively, this variation within a device was smaller than that between devices (SD = 3.9 μm, 23%). In comparing the average thicknesses between devices, it is noted that this variation is large enough so that all three devices produced biofilms significantly different from each other (P -value < 0.05). The average thickness of all points measured over all devices is 16.5 μm, with a 3.5 μm (21%) standard deviation. Using an unweighted analysis of variance, the variance between devices was 9.82 μm² (standard error [SE] 2.25, P -value 0.8388), and the variance within a device between measurement locations was 0.61 μm² (SE 0.67, P -value 0.0006). The smaller differences in average thickness over one channel as compared between the three devices highlight the importance of an integrated control. These results confirm that the biofilms are uniform throughout the central channel of each device, and have more uniform thicknesses than biofilms grown between devices.

The results of this thickness uniformity study are analogous to results obtained in other single channel, single depth microfluidic devices. An example of one such set of results obtained using four devices tested in parallel is provided in supplementary material, figure S4 (stacks.iop.org/JMM/25/095003/mmedia). Similar to the uniformity study in branched, valved microfluidic devices, the thickness variation within each single-channel device (SD < 3 μm, 16% of the average thickness at greatest) was less than that between devices (SD = 14.9 μm, 75%). The observation of large variation in biofilms formed in separate devices tested

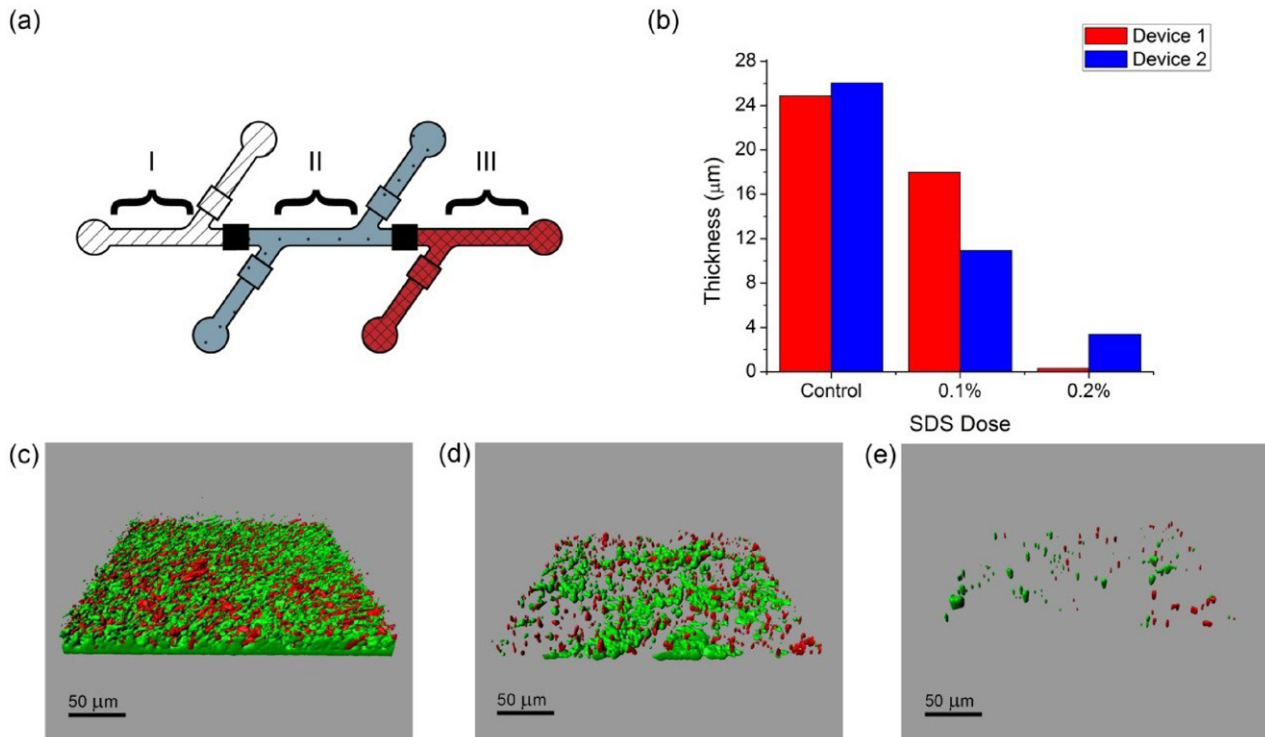


Figure 6. (a) Schematic of device operation during biofilm segmentation, with the central channel trisected by two closed valves. Confocal microscopy images were obtained at the center of each of the three sections indicated (I, II, and III) (b) Average biofilm thicknesses measured at the imaged locations in the two tested devices with different SDS exposure levels. (c)–(e) Surface rendered confocal microscopy images of *E. coli* biofilms in Device 1 with (c) no treatment (control) (d) exposure to 0.1% SDS, and (e) exposure to 0.2% SDS. Biofilm thicknesses were 24.9, 7.9, and 0.3 μm respectively.

in parallel, regardless of geometry, supports the need for controls to be integrated within each microfluidic device in order to ensure reliable comparison and evaluation of biofilm treatments.

While biofilm thickness is a frequently used parameter for evaluating the state of a biofilm, a greater understanding of biofilms may be gained using additional metrics such as biomass or substratum coverage [37]. Biofilm uniformity in the valved devices was analyzed in terms of biomass and substratum coverage, and these data are presented in supplementary material, figure S5 (stacks.iop.org/JMM/25/095003/mmedia). In comparing the averaged biomass between devices, it is noted that the biofilms formed in Devices 1 and 2 were not significantly different from each other (P -value 0.6811), but the biofilm formed in Device 3 had a significantly different biomass (P -value < 0.05) from Devices 1 and 2. Substratum coverage was also only significantly different between Devices 2 and 3 (P -value < 0.05), while Device 1 did not produce a significantly different substratum coverage from either Device 2 or 3 (P -value 0.3623 and P -value 0.1094, respectively). The variation of biomass within each device ($\text{SD} = 1.7 \mu\text{m}^3 \mu\text{m}^{-2}$ at greatest) was comparable to the variation between devices ($\text{SD} = 2.1 \mu\text{m}^3 \mu\text{m}^{-2}$). Variation of substratum coverage within each device ($\text{SD} = 11.5\%$ at greatest) was also similar to the variation of substratum coverage between devices ($\text{SD} = 10.5\%$). Considering these observations, the parameters of biomass and substratum coverage appear to have little dependence on whether the measurements are pooled from one biofilm in one

microfluidic channel, or several biofilms formed in different devices.

3.3. Biofilm segmentation

The applicability of the device toward biofilm studies was demonstrated by testing biofilm sensitivity to SDS within a single device. SDS is an anionic surfactant that has been shown to denature the bacterial cell wall by solubilizing its phospholipid and protein contents [38, 39]. Exposure of bacterial biofilms to SDS has been used as a gauge of biofilm health [40], as well as a method for preventing biofilm formation [41]. After growing *E. coli* biofilms for 60h, the valve orientation was switched, dividing the central channel into three sections, as depicted in figures 1(b) and 4(b). The three biofilm sections were either treated with 0.1% or 0.2% SDS, or remained untreated as a control. Two devices were tested in parallel; the location of each treatment within the device (i.e. section I, II, or III as pictured in figure 6(a)) was varied between the devices as described in table 1. Thickness results from the segmentation studies are summarized in figure 6(b), and samples of rendered confocal microscopy images from one of the devices are presented in figures 6(c)–(e). In both devices, the control biofilm was thickest, and increasing the SDS concentration decreased the measured thickness in the applicable segment. Additionally, there appears to be no relationship between location of treatment administration and the results obtained; despite administration of treatments to

Table 1. Summary of treatments applied to biofilm sections in each device, describing how positioning of treatments was varied between the two devices tested. Section I denotes the section closest to the inlet, and III denotes the section closest to the outlet.

Section	Treatment	
	Device 1	Device 2
I	Control	0.1% SDS
II	0.1% SDS	0.2% SDS
III	0.2% SDS	Control

biofilm segments at different locations within the device, both devices show similar trends for thickness versus SDS concentration. This observation relies on the observed biofilm uniformity within the channel (figure 5), which enables the assumption that the control segment represents state the biofilms in the other two segments would have achieved if not for SDS exposure. The results demonstrate the use of microfluidic devices to perform multiple, controlled experiments on a single biofilm.

4. Discussion

This work has two major contributions: the concept of a microfluidic device with an integrated biofilm control, and the photoresist passivation technology used to create this device. The device itself features integrated valves to section biofilms grown in microfluidics. This was accomplished via a novel fabrication method addressing the differing depth requirements for valves and biofilms by patterning multiple layers of photoresist with ALD-deposited passivation in between layers.

This fabrication technique was used to create an unprecedented device for parallel biofilm studies. The developed microfluidic platform addresses the issue of intrinsic variability in biofilms. While the variability can partially be addressed by performing an experiment multiple times and examining data trends, implementing internal controls adds an additional level of scientific rigor. While variation in biomass and substratum coverage was comparable between devices, the need for internal controls is clear in the device-to-device variation of biofilm thickness in this work. In this demonstration of the valved biofilm sectioning device, within-device biofilm variation was less than between-device variation. By comparing sections of one biofilm grown in one device, fewer iterations of an experiment would be required to obtain a representative understanding of the biofilm phenomena at play than if biofilms were grown in and compared between separate devices. Expansion of the device design to include more biofilm sections than the three demonstrated in this work will also allow more experiments to be performed in the same platform. These experiments could range from the identification of appropriate staining procedures to the evaluation of biofilm sensitivity to antibiotics or shear stress.

In order to create the device presented here, a new fabrication process for protecting photoresist from chemical attack by solvents was developed. The use of ALD to deposit

chemically passivating barriers on photoresist reliably allowed patterned resist to withstand further photolithographic processing. This capability is particularly of interest since it enables creation of unique architectures in PDMS, such as the multi-profile microchannels in this work, which might otherwise be more difficult and costly to create using other PDMS molding methodologies. ALD can be used to passivate a multitude of photoresists or other polymeric materials with different patterning capabilities or thicknesses to create varied microchannel geometries. As the body of research on ALD processing expands, there are an increasing number of methods for low-temperature deposition of a variety of materials [31, 42], which in turn may be used for passivating polymers more sensitive to high temperatures. The ability to deposit very thin layers of high quality material facilitates the creation of even finer passivated photoresist patterns than those demonstrated here (on the order of $100\ \mu\text{m}$). Using ALD passivation allows researchers the freedom to use any polymeric materials regardless of compatibility.

The fabrication technology of ALD passivation of photoresist to create multi-depth, multi-profile microfluidics also can be applied to an even broader number of applications even outside the field of bacterial biofilms. Microfluidics with mixed profiles can be applied to the growing number of tissue culture studies in microenvironments [14, 43]. Multi-depth microfluidics would also be useful in hydrodynamic studies where the channel dimensions would affect the results [44].

This work features hydraulically actuated PDMS push-up valves, with the control channel and spun-on membrane as the bottom-most PDMS layer and the multi-depth channel on top; this configuration entails biofilm growth on top of a PDMS substrate. The device presented here is suited for inverted confocal microscopy imaging, as the light path must only pass through the coverslip and the bottom-most PDMS layer before encountering the biofilm. While using confocal microscopy is a standard method for biofilm observation and quantification [45], more information about biofilms can be gathered in a continuous manner by integrating sensors into the microfluidic platform. As the biofilm grows on top of PDMS, integration of electrical or mechanical sensors would require sensor fabrication within or on top of the PDMS [46, 47], or integration of pre-fabricated sensors into the PDMS [48, 49]. While possible, these processes may require extensive characterization so that the sensor integration fabrication processes do not preclude valve operation. The device is immediately compatible with off-chip, continuous optical detection methods such as optical density [20, 50] or on-chip fluorescence [51]. The integrated hydraulic valves featured in this work allow the entire device to remain compact and to be integrated without opaque instrumentation impeding lightpaths. Expanding this methodology to include integrated biofilm optical density measurement for continuously evaluating the biofilm state will provide additional information unattainable with end-point measurements from microscopy [20, 50]. For instance, any instantaneous changes in the biofilm structure can be measured as the valve orientations are switched for biofilm sectioning. Real-time biofilm sensitivity to antibiotics can also be measured, offering more detailed

information about antibiotic tolerance kinetics than end-point microscopy can provide.

5. Conclusions

Microfluidics provide a convenient platform for targeting the challenge of bacterial biofilms, enabling scientific studies and drug testing in a small format easily integrated with many sensing modalities. We address the issue of biofilm variability between microfluidic devices by creating a platform where one biofilm is grown and sectioned into discrete segments that can each be subjected to different treatments in parallel or used as internal controls. Sectioning is achieved using hydraulic valves integrated with a two-depth biofilm growth channel, enabled by ALD passivation of a photoresist mold to bypass incompatibilities between multiple photoresists. The platform was successfully used to segment biofilms and evaluate sensitivity to SDS. In this work, we observed the need for integrated controls in biofilm studies and how the presented platform addresses this need. The novel ALD passivation technology developed to enable this work has an even broader impact beyond the biofilm research community, as photoresist passivation enables a host of microfluidic devices with varied cross-sectional geometries. Our work introduces an additional degree of freedom in channel geometry into the microfluidic toolbox, thereby expanding experimental design options as well as the broader base of scientific knowledge produced by microfluidic technologies.

Acknowledgments

The authors appreciate the funding support provided by the Robert W Deutsch Foundation, the National Science Foundation (CBET #1160005, CBET #1264509), and the Defense Threat Reduction Agency (HDTRA1-13-1-00037). The authors appreciate the support of the Maryland Nanocenter and its Fablab in fabricating the microfluidic devices and also appreciate the assistance of the University of Maryland Imaging Core Facility with confocal microscopy. They would additionally like to thank Dr Nathan Siwak and Dr Xiao Zhu Fan for assistance with obtaining scanning electron microscopy images, and their collaborators in the University of Maryland Biochip Collaborative for useful discussions.

References

- [1] Bordi C and de Bentzmann S 2011 Hacking into bacterial biofilms: a new therapeutic challenge *Ann. Intensive Care* **1** 19
- [2] Fux C A, Stoodley P, Shirliff M and Costerton J W 2009 The functional resistance of bacterial biofilms *Antimicrobial Drug Resistance* ed D L Mayers (New York: Humana Press) pp 121–31
- [3] Richards J J and Melander C 2009 Controlling bacterial biofilms *Chem. Bio Chem.* **10** 2287–94
- [4] Hoiby N, Ciofo O, Johansen H K, Song Z J, Moser C, Jensen P O, Molin S, Givskov M, Tolker-Nielsen T and Bjarnsholt T 2011 The clinical impact of bacterial biofilms *Int. J. Oral Sci.* **3** 55–65
- [5] Ceri H, Olson M E, Stremick C, Read R R, Morck D and Buret A 1999 The calgary biofilm device: new technology for rapid determination of antibiotic susceptibilities of bacterial biofilms *J. Clin. Microbiol.* **37** 1771–6
- [6] Cruz S A, Popat R, Rybtke M T, Camara M, Givskov M, Tolker-Nielsen T, Diggle S P and Williams P 2012 Bursting the bubble on bacterial biofilms: a flow cell methodology *Biofouling* **28** 835–42
- [7] Gilmore B F, Hamill T M, Jones D S and Gorman S P 2010 Validation of the CDC biofilm reactor as a dynamic model for assessment of encrustation formation on urological device materials *J. Biomed. Mater. Res. B-Appl. Biomater.* **93B** 128–40
- [8] Kharazmi A, Giwercman B and Hoiby N 1999 Robbins device in biofilm research *Methods Enzymol.* **310** 207–15
- [9] Heydorn A, Ersbøll B K, Hentzer M, Parsek M R, Givskov M and Molin S 2000 Experimental reproducibility in flow-chamber biofilms *Microbiology* **146** 2409–15 (PMID: 11021917)
- [10] Roeselers G, Zippel B, Staal M, van Loosdrecht M and Muyzer G 2006 On the reproducibility of microcosm experiments—different community composition in parallel phototrophic biofilm microcosms *Fems Microbiol. Ecol.* **58** 169–78
- [11] Djeribi R, Bouchloukh W, Jouenne T and Mena B 2012 Characterization of bacterial biofilms formed on urinary catheters *Am. J. Infect. Control* **40** 854–9
- [12] Rochex A, Godon J-J, Bernet N and Escudie R 2008 Role of shear stress on composition, diversity and dynamics of biofilm bacterial communities *Water Res.* **42** 4915–22
- [13] Yin H and Marshall D 2012 Microfluidics for single cell analysis *Curr. Opin. Biotechnol.* **23** 110–9
- [14] Polacheck W J, Li R, Uzel S G and Kamm R D 2013 Microfluidic platforms for mechanobiology *Lab Chip* **13** 2252–67
- [15] Velve-Casquillas G, Le Berre M, Piel M and Tran P T 2010 Microfluidic tools for cell biological research *Nano Today* **5** 28–47
- [16] Kim J, Kim H-S, Han S, Lee J-Y, Oh J-E, Chung S and Park H-D 2013 Hydrodynamic effects on bacterial biofilm development in a microfluidic environment *Lab Chip* **13** 1846–9
- [17] Hong S H, Hegde M, Kim J, Wang X, Jayaraman A and Wood T K 2012 Synthetic quorum-sensing circuit to control consortial biofilm formation and dispersal in a microfluidic device *Nat. Commun.* **3** 613
- [18] Janakiraman V, Englert D, Jayaraman A and Baskaran H 2009 Modeling growth and quorum sensing in biofilms grown in microfluidic chambers *Ann. Biomed. Eng.* **37** 1206–16
- [19] Kim J, Hegde M, Kim S H, Wood T K and Jayaraman A 2012 A microfluidic device for high throughput bacterial biofilm studies *Lab Chip* **12** 1157–63
- [20] Meyer M T, Roy V, Bentley W E and Ghodssi R 2011 Development and validation of a microfluidic reactor for biofilm monitoring via optical methods *J. Micromech. Microeng.* **21** 054023
- [21] Roy V, Meyer M, Smith J I, Gamby S, Sintim H, Ghodssi R and Bentley W 2013 AI-2 analogs and antibiotics: a synergistic approach to reduce bacterial biofilms *Appl. Microbiol. Biotechnol.* **97** 2627–38
- [22] Kim K P, Kim Y G, Choi C H, Kim H E, Lee S H, Chang W S and Lee C S 2010 *In situ* monitoring of antibiotic susceptibility of bacterial biofilms in a microfluidic device *Lab Chip* **10** 3296–9
- [23] Zhang Q, Lambert G, Liao D, Kim H, Robin K, Tung C-K, Pourmand N and Austin R H 2011 Acceleration of emergence of bacterial antibiotic resistance in connected microenvironments *Science* **333** 1764–7

- [24] Kim J, Park H D and Chung S 2012 Microfluidic approaches to bacterial biofilm formation *Molecules* **17** 9818–34
- [25] El-Ali J, Sorger P K and Jensen K F 2006 Cells on chips *Nature* **442** 403–11
- [26] Hulme S E, Shevkopylas S S and Whitesides G M 2009 Incorporation of prefabricated screw, pneumatic, and solenoid valves into microfluidic devices *Lab Chip* **9** 79–86
- [27] Melin J and Quake S R 2007 Microfluidic large-scale integration: the evolution of design rules for biological automation *Annu. Rev. Biophys. Biomol. Struct.* **36** 213–31
- [28] Studer V, Hang G, Pandolfi A, Ortiz M, Anderson W F and Quake S R 2004 Scaling properties of a low-actuation pressure microfluidic valve *J. Appl. Phys.* **95** 393–8
- [29] Thorsen T, Maerkl S J and Quake S R 2002 Microfluidic large-scale integration *Science* **298** 580–4
- [30] Xia Y N and Whitesides G M 1998 Soft lithography *Annu. Rev. Mater. Sci.* **28** 153–84
- [31] George S M 2010 Atomic layer deposition: an overview *Chem. Rev.* **110** 111–31
- [32] Leskelä M and Ritala M 2002 Atomic layer deposition (ALD): from precursors to thin film structures *Thin Solid Films* **409** 138–46
- [33] Sinha A, Hess D W and Henderson C L 2006 A top surface imaging method using area selective ALD on chemically amplified polymer photoresist films *Electrochem. Solid-State Lett.* **9** G330–G3
- [34] Biercuk M J, Monsma D J, Marcus C M, Becker J S and Gordon R G 2003 Low-temperature atomic-layer-deposition lift-off method for microelectronic and nanoelectronic applications *Appl. Phys. Lett.* **83** 2405–7
- [35] Färm E, Kemell M, Santala E, Ritala M and Leskelä M 2010 Selective-area atomic layer deposition using Poly(vinyl pyrrolidone) as a passivation layer *J. Electrochem. Soc.* **157** K10–K4
- [36] Eddings M A, Johnson M A and Gale B K 2008 Determining the optimal PDMS–PDMS bonding technique for microfluidic devices *J. Micromech. Microeng.* **18** 067001
- [37] Heydorn A, Nielsen A T, Hentzer M, Sternberg C, Givskov M, Ersboll B K and Molin S 2000 Quantification of biofilm structures by the novel computer program COMSTAT *Microbiology* **146** 2395–407 (PMID: [11021916](#))
- [38] Gawande P, LoVetri K, Yakandawala N, Romeo T, Zhanel G, Cvitkovitch D and Madhyastha S 2008 Antibiofilm activity of sodium bicarbonate, sodium metaperiodate and SDS combination against dental unit waterline-associated bacteria and yeast *J. Appl. Microbiol.* **105** 986–92
- [39] O'Toole G A, Pratt L A, Watnick P I, Newman D K, Weaver V B and Kolter R 1999 *Methods in Enzymology* ed J D Ron (New York: Academic) pp 91–109
- [40] Davies D G, Parsek M R, Pearson J P, Iglewski B H, Costerton J W and Greenberg E P 1998 The involvement of cell-to-cell signals in the development of a bacterial biofilm *Science* **280** 295–8
- [41] Li L, Molin S, Yang L and Ndoni S 2013 Sodium dodecyl sulfate (SDS)-loaded nanoporous polymer as anti-biofilm surface coating material *Int. J. Mol. Sci.* **14** 3050–64
- [42] Knez M, Niesch K and Niinistö L 2007 Synthesis and surface engineering of complex nanostructures by atomic layer deposition *Adv. Mater.* **19** 3425–38
- [43] Lee J-H, Wang H, Kaplan J B and Lee W Y 2011 Microfluidic approach to create 3D tissue models for biofilm-related infection of orthopaedic implants *Tissue Eng. C-Methods* **17** 39–48
- [44] Ben-Yoav H, Dykstra P H, Bentley W E and Ghodssi R 2012 A microfluidic-based electrochemical biochip for label-free diffusion-restricted DNA hybridization analysis *Biosensors Bioelectron.* **38** 114–20
- [45] Pantanella F, Valenti P, Natalizi T, Passeri D and Berlutti F 2013 Analytical techniques to study microbial biofilm on abiotic surfaces: pros and cons of the main techniques currently in use *Annali di igiene: medicina preventiva e di comunità* **25** 31–42
- [46] Paranjape M, Garra J, Brida S, Schneider T, White R and Currie J 2003 A PDMS dermal patch for non-invasive transdermal glucose sensing *Sensors Actuators A: Phys.* **104** 195–204
- [47] Wu W-Y, Zhong X, Wang W, Miao Q and Zhu J-J 2010 Flexible PDMS-based three-electrode sensor *Electrochem. Commun.* **12** 1600–4
- [48] Lu N, Lu C, Yang S and Rogers J 2012 Highly sensitive skin-mountable strain gauges based entirely on elastomers *Adv. Funct. Mater.* **22** 4044–50
- [49] Reina A, Son H, Jiao L, Fan B, Dresselhaus M S, Liu Z and Kong J 2008 Transferring and Identification of single- and few-layer graphene on arbitrary substrates *J. Phys. Chem. C* **112** 17741–4
- [50] Kim Y W, Mosteller M P, Meyer M T, Ben-Yoav H, Bentley W E and Ghodssi R 2012 Microfluidic biofilm observation, analysis, and treatment (Micro-BOAT) platform *Solid-State Sensors, Actuators and Microsystems Workshop (Hilton Head Workshop 2012) (Hilton Head, SC, USA)* pp 233–6
- [51] Ateya D A, Erickson J S, Howell P B, Hilliard L R, Golden J P and Ligler F S 2008 The good, the bad, and the tiny: a review of microflow cytometry *Anal. Bioanal. Chem.* **391** 1485–98